



Effects of simultaneous carrier doping in the charge reservoir and conducting layers of superconducting $\text{CeO}_{0.9}\text{F}_{0.1}\text{Fe}_{1-x}\text{Co}_x\text{As}$

S.J. Singh^a, J. Prakash^b, S. Patnaik^{a,*}, A.K. Ganguli^{b,**}

^a School of Physical Sciences, Jawaharlal Nehru University, New Delhi 110 067, India

^b Department of Chemistry, Indian Institute of Technology, New Delhi 110 016, India

ARTICLE INFO

Article history:

Received 24 June 2010

Accepted 22 July 2010

Available online 25 July 2010

Keywords:

Iron-based superconductor

Electronic transport and superconducting gap

ABSTRACT

Electron-doping of the semimetal (CeOFeAs) by either fluorine (max $T_c \sim 43$ K) or cobalt (max $T_c \sim 11$ K) leads to superconductivity. Here we show the effect of transition metal (Co) substitution at the iron site on the superconducting properties of $\text{CeO}_{0.9}\text{F}_{0.1}\text{FeAs}$ ($T_c \sim 38$ K) to understand the interplay of charge carriers in both the rare earth-oxygen and Fe–As layers. Simultaneous doping of equivalent number of charge carriers in both layers leads to a T_c of 9.8 K which is lower than the T_c obtained when either the conducting layer (FeAs) or charge reservoir layer (CeO) is individually doped. This suggests a clear interplay between the two layers to control the superconductivity. Resistivity upturn and negative magnetoresistance are observed with Co doping that is interpreted in the gamut of Kondo effect. Hall coefficient and thermoelectric power indicate increased carrier concentration with cobalt doping in $\text{CeO}_{0.9}\text{F}_{0.1}\text{FeAs}$. The rf penetration depth both for $\text{CeO}_{0.9}\text{F}_{0.1}\text{Fe}_{0.95}\text{Co}_{0.05}\text{As}$ and $\text{CeO}_{0.9}\text{F}_{0.1}\text{FeAs}$ show an exponential temperature dependence with gap values of ~ 1.6 and 1.9 meV respectively.

© 2010 Elsevier B.V. All rights reserved.

1. Introduction

Superconductivity in the ferropnictides has provided a novel opportunity for a deeper understanding of the mechanism of high temperature superconductivity in the presence of competing magnetic and superconducting correlations. Consequently, there have been several efforts to draw a parallel between the high T_c cuprates and ferropnictides [1,2]. It has now been established that unlike cuprates, where the ground state is a Mott Insulator with superexchange linked local moments at copper sites, the oxypnictides are (semi)metallic with effectively very weak magnetism as evidenced by a spin density wave correlation. Band structure calculations and photoelectron spectroscopic studies have revealed itinerant characteristics of Fe 3d electrons [2]. Further, amongst the ferropnictides, the Ce(O/F)FeAs (max $T_c \sim 43$ K, $x = 0.2$) system is unique because of striking similarity [3] of the electronic phase diagram with cuprates, notably a dome-shaped T_c dependence on carrier doping [4]. The parent oxypnictide, CeOFeAs, undergoes a structural phase transition from tetragonal ($P4/nmm$) to orthorhombic ($Cmma$) structure around 155 K followed by an antiferromagnetic ordering of spins in the Fe sublattice at ~ 140 K. From detailed neutron scattering measurements it is now established that upon F doping in $\text{CeO}_{1-x}\text{F}_x\text{FeAs}$, both AFM ordering and the structural phase transition

vanishes at $x > 0.06$ leading to superconductivity [4]. Most strikingly, it has been shown that instead of F at O sites, Co doping at Fe sites in LnOFeAs can also induce superconductivity [5,6]. This is instructive because LaOCoAs is a metal that becomes a ferromagnet at 66 K [7]. All the above properties indicate that magnetic fluctuations play a critical role in the stabilization of the superconducting state in ferropnictides. To get further insight into the electronic correlation effects of the FeAs layer, we have chosen to dope the iron sites with cobalt in the superconducting composition ($\text{CeO}_{0.9}\text{F}_{0.1}\text{FeAs}$) where the AFM (SDW) state has already been suppressed by F doping. In the undoped CeOFeAs, the nearest neighbor and next nearest neighbor interactions are superexchange controlled and lead to a frustrated stripelike AFM state [4]. Wang et al. [5] reported the superconductivity in cobalt-doped LnOFeAs (Ln = La and Sm) where cobalt doping at Fe sites leads to a double exchange interaction between Fe and Co sites [5]. Thus the role of Co doping in optimally doped $\text{CeO}_{0.9}\text{F}_{0.1}\text{FeAs}$ is two fold; to overdope carriers onto the FeAs (conducting) layers and to introduce disorder in the Fe antiferromagnetic order (dormant due to F doping). In this paper we report studies on resistivity, magnetoresistance, Hall effect, thermoelectric power and rf penetration depth of such a optimally doped series of oxypnictide specimen undergoing simultaneous addition of charge carriers with local magnetic moments.

2. Experimental

Polycrystalline samples with nominal compositions of $\text{CeO}_{0.9}\text{F}_{0.1}\text{Fe}_{1-x}\text{Co}_x\text{As}$ with 'x' = 0.05, 0.10 and 0.15 were synthesized by a two

* Corresponding author. Tel.: +91 11 26704783; fax: +91 11 26717537.

** Corresponding author.

E-mail addresses: spatnaik@mail.jnu.ac.in (S. Patnaik), ashok@chemistry.iitd.ernet.in (A.K. Ganguli).

step solid state reaction method [8] using high purity Ce, CeO₂, CeF₃, Co₃O₄, As and FeAs as starting materials. FeAs was obtained by reacting Fe chips and As powder at 800 °C for 24 h. The raw materials (all with purities better than 99.9%) were taken according to stoichiometric ratio and then sealed in evacuated silica ampoules (10⁻⁴ torr) and heated at 950 °C for 24 h. The powder was then compacted (5 tonnes) and the disks were wrapped in Ta foil, sealed in evacuated silica ampoules and heated at 1150 °C for 48 h. All chemicals were handled in a nitrogen-filled glove box. The resulting samples were characterized by powder X-ray diffraction (PXRD) with Cu K α radiation. The lattice parameters were obtained using a least squares fit to the observed *d* values.

Resistivity, Hall effect and rf susceptibility measurements were carried out using a cryogenic 8 T cryogen-free magnet in conjunction with a variable temperature insert (VTI). Standard four probe technique was used for transport measurements. The external magnetic field (0–3 T) was applied perpendicular to the probe current direction and the data were recorded during the warming cycle with heating rate of 1 K/min. The inductive part of the magnetic susceptibility was measured using a tunnel diode based rf penetration depth technique [9]. The sample was kept inside an inductor that formed a part of an LC circuit of an ultrastable oscillator (~2.3 MHz). A change in the magnetic state of the sample results in a change in the inductance of the coil and is reflected as a shift in oscillator frequency which is measured by an Agilent 53131A counter. The thermoelectric power measurement of each sample was carried out by bridge geometry where a temperature gradient was created across a 2 mm by 3 mm rectangular disk.

3. Results and discussion

Fig. 1(i) shows the PXRD patterns of CeO_{0.9}F_{0.1}Fe_{1-x}Co_xAs (*x* = 0.05, 0.10 and 0.15) compounds. The observed reflections could be satisfactorily indexed on the basis of a tetragonal ZrCu-SiAs type structure. Fig. 1(ii) shows the variation of lattice parameters as a function of Co content. With increasing Co content (*x*), the '*a*'-axis goes down marginally while the '*c*'-axis shrinks significantly indicating successful incorporation of cobalt ions (the ionic size of cobalt(II) is smaller than that of iron(II)).

The zero field resistivity plots between 1.6 K and 300 K for CeO_{0.9}F_{0.1}Fe_{1-x}Co_xAs (Fig. 2) show metallic behavior in the normal state. The sample without Co doping (CeO_{0.9}F_{0.1}FeAs) shows the superconducting transition at around 38.5 K [10]. With Co doping, the onset of superconducting transition decreased to 23.4 and 9.8 K for (a) CeO_{0.9}F_{0.1}Fe_{0.95}Co_{0.05}As and (b) CeO_{0.9}F_{0.1}Fe_{0.9}Co_{0.1}As respectively (Fig. 2). The diamagnetic behavior of these superconductors was confirmed from the susceptibility studies which are shown in Fig. 7. On increasing the Co content (*x* = 0.15) further the *T_c* decreases dramatically and only a steep drop in the resistivity around 4 K (Fig. 3d) was observed (zero resistance state could not be achieved down to 1.6 K). The residual resistivity value (RRR = ρ_{300}/ρ_{25}) is 5.8 and 2.11 for *x* = 0.05 and 0.10 compositions respectively (RRR = 4.34 for CeO_{0.9}F_{0.1}FeAs [10]) indicate increase in disorder with Co doping. It is to be noted that while in the compositions without fluorine CeOFe_{1-x}Co_xAs, both the transition temperature and $\rho(T_c)$ always decreased with increasing *x* > 0.01 [6], on the contrary we observe that $\rho(T_c)$ first increases with Co doping but reduces drastically for *x* ~ 0.15 and shows dome like behavior (optimal dopant concentration exists). This is reminiscent of distinctly different transport behavior in the metallic regions of LaO_{1-x}F_xFe_{1-y}Co_yAs (*x* = 0.1) [11]. Various studies have shown that optimal *T_c* in all oxypnicted superconductors depends on the presence of ideal (undistorted) FeAs₄ tetrahedra (bond angle of 109° 28') [4]. The decrease in *T_c* on Co doping at Fe site in CeO_{0.9}F_{0.1}Fe_{1-x}Co_xAs may be related to increase in the Fe–As–Fe angle

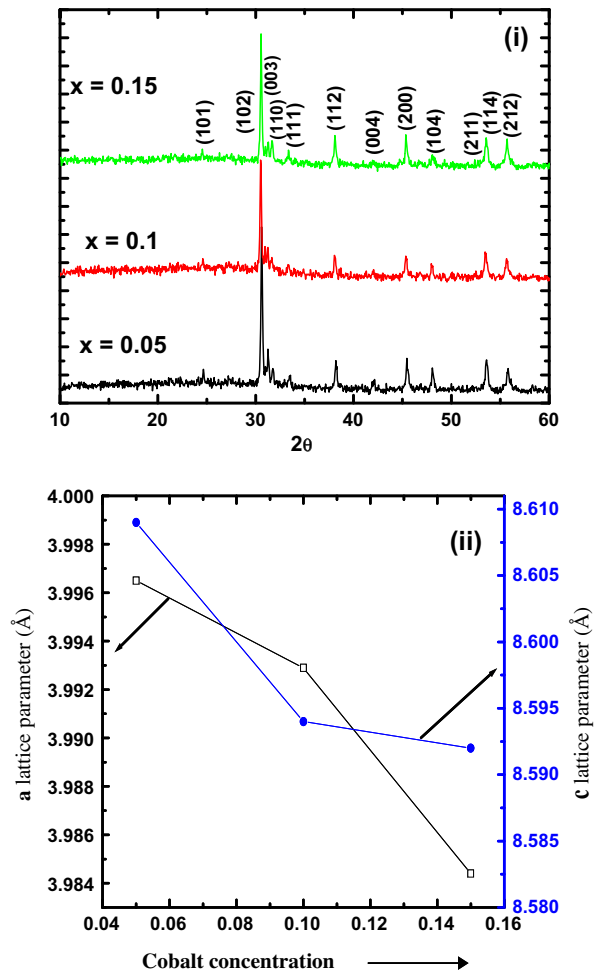


Fig. 1. (i) Powder X-ray diffraction patterns (PXRD) of CeO_{0.9}F_{0.1}Fe_{1-x}Co_xAs (*x* = 0.05, 0.10 and 0.15). (ii) The variation of the lattice parameters (*a* and *c*) on the Co content (*x*) for CeO_{0.9}F_{0.1}Fe_{1-x}Co_xAs.

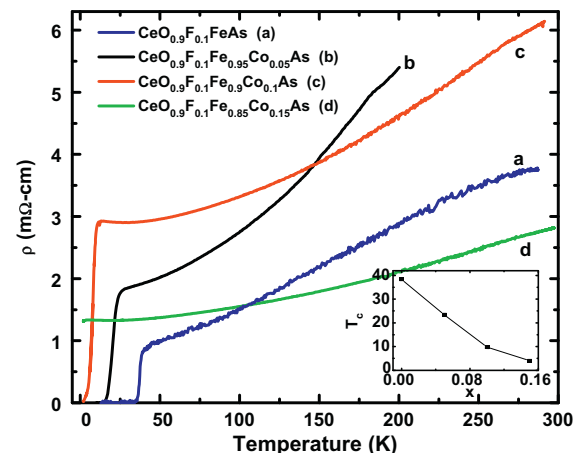


Fig. 2. The temperature dependence of resistivity (ρ) as a function of temperature for CeO_{0.9}F_{0.1}Fe_{1-x}Co_xAs (*x* = 0, 0.05, 0.10 and 0.15). Inset shows the dependence of transition temperature (*T_c*) with Co content (*x*).

though the interlayer distance between CeO/F and FeAs layers decreases by doping Co in place of Fe. Our results are in line with what is seen in LaO(Fe/Co)As, where the Fe–As–Fe bond angle increases with Co doping [5]. This reinforces the understanding that Fe–As–Fe bond angles play a dominant role in determining the

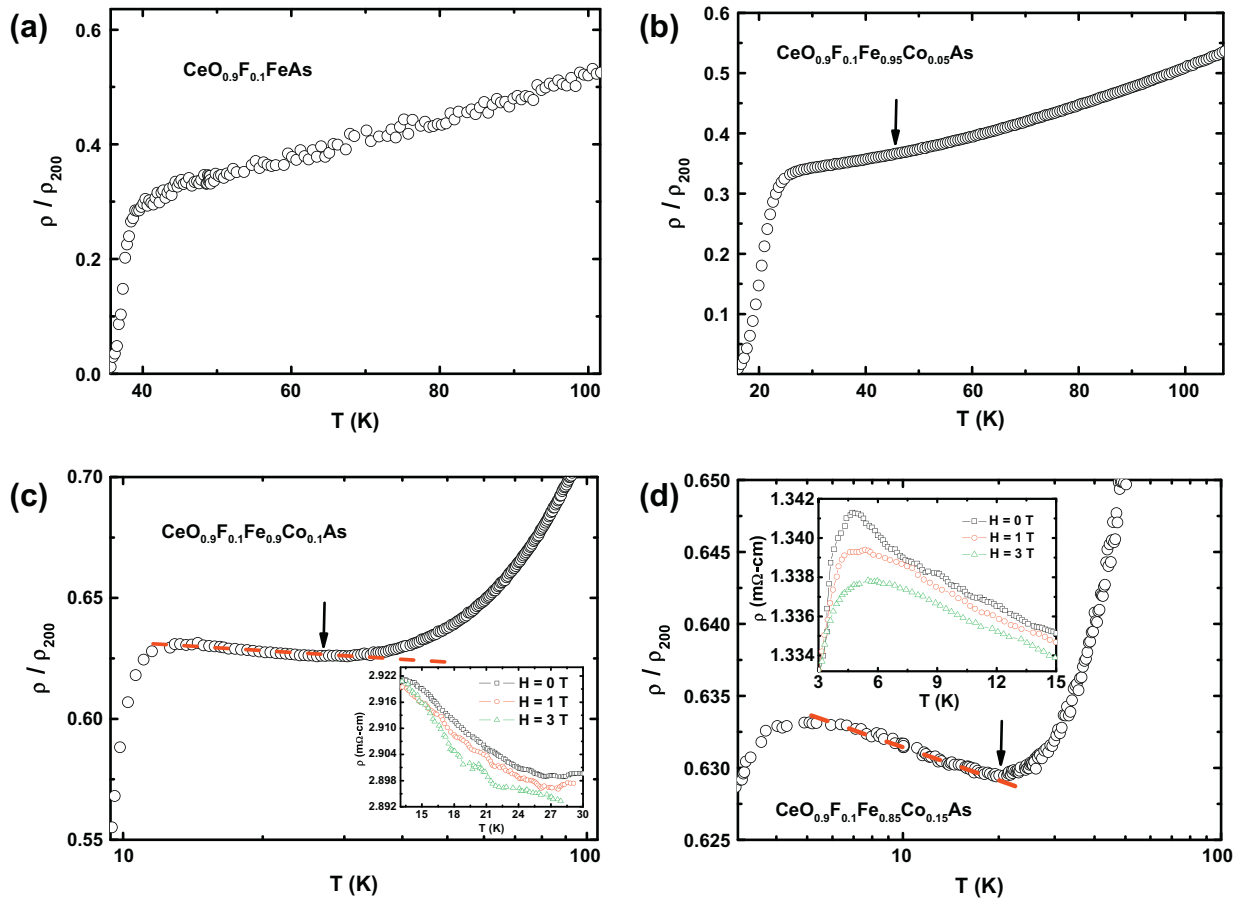


Fig. 3. The normalized resistivity with respect to temperature variation for $\text{CeO}_{0.9}\text{F}_{0.1}\text{Fe}_{1-x}\text{Co}_x\text{As}$ series, in figure (c) and (d) temperature scale in $\log(T)$. Inset of figure (c) and (d) show the negative magnetoresistance for $x = 0.10$ and $x = 0.15$. Arrows show the minimum point (T_{\min}) and the red dashed lines are linear fit. (For interpretation of the references to colour in this figure legend, the reader is referred to the web version of this article.)

optimal T_c , more than the decreasing distances between the reservoirs and conducting layers.

Fig. 3 shows the evolution of the temperature dependence of normal state resistivity as a function of Co doping. We find a striking increase in $\rho(T_c)$ with cobalt doping for $x < 0.15$ and a resistivity minimum followed by an upturn as shown in Fig. 3a–d. When we increased the Co concentration in $\text{CeO}_{0.9}\text{F}_{0.1}\text{FeAs}$, this upturn temperature T_{\min} shifted to lower temperature. Weak localization or Kondo effect could be invoked towards explaining this upturn [12]. As plotted in the inset of Fig. 3c and d we also observe sign change in magnetoresistance (MR) that give credence to the interpretation that the resistivity upturn is due to spin flip scattering between the charge carriers and local Co moments. Further, the x -axis in 3c and 3d are set to \log scale and the dashed line indicates robust $\log(1/T)$ behavior as expected for a Kondo system. The width of $\log(T)$ area decreases with increasing Co fraction. Such behavior has also been seen in Ni doped LaOFeAs [13] and Rh doped NdFeAsO systems [14].

To understand the effective carrier concentration in this optimally doped series of a multiband superconductor (upon addition of Co), in Figs. 4 and 5 we plot Hall and thermoelectric power data, respectively. While for a metal the variation of Hall coefficient (R_H) with temperature remains nearly invariant with temperature, it exhibits temperature dependent behavior for a multiband material such as MgB_2 [15] or materials with non-Fermi liquid behavior such as the cuprates [16]. As shown in Fig. 4a, we find that the transverse resistivity (ρ_{xy}) remains negative up to room temperature for all the compositions. This indicates that in spite of multiple

hole and electron pockets, the transport is dominated by electrons. We find that the slope of ρ_{xy} vs. H decreases with increasing cobalt concentration. This indicates that carrier concentration increases with the substitution of cobalt (in place of iron) in this optimally doped superconductor $\text{CeO}_{0.9}\text{F}_{0.1}\text{FeAs}$.

The thermopower (S) as a function of temperature for the parent compound CeOFeAs is shown in Fig. 5. In the high temperature region (200–300 K), S was observed to be negative (suggesting electrons to be the majority charge carriers), and its value increased linearly as a function of temperature. A linear dependence of the thermopower (S) is a signature of metallic behavior which reaches a minimum (T_{\min}) around 170 K for the parent compound CeOFeAs as that reported previously [17]. On further cooling, the thermopower increases. The Co-doped compositions ($\text{CeO}_{0.9}\text{F}_{0.1}\text{Fe}_{1-x}\text{Co}_x\text{As}$) also show a negative value of the thermopower (Fig. 5). For $\text{CeO}_{0.9}\text{F}_{0.1}\text{FeAs}$ (without Co doping) as shown in Fig. 5, the Seebeck coefficient varies from $-22 \mu\text{V/K}$ at 300 K to a value of $\sim -104 \mu\text{V/K}$ at ~ 60 K. The Co-doped samples have similar room temperature value but a much weaker minima and then sharp increase as the temperature is lowered further. Thus the absolute value of thermopower decreases with increasing Co doping. In a minimal two band model [18], the conductivity and thermopower depend on hole and electron contributions, and therefore while it is certain that with cobalt doping the conduction mechanism is dominated by electrons, the sharp increase in thermopower is due to contribution of holes in the over-doped regime.

To obtain the upper critical field (H_{c2}), we have compared the temperature dependence of the resistivity under varying magnetic

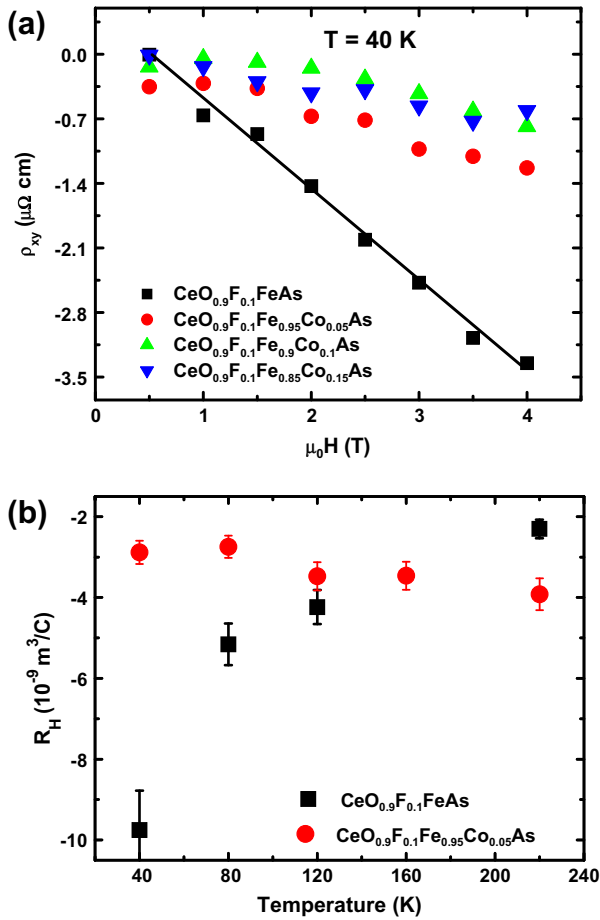


Fig. 4. (a) Hall resistivity as a function of field and (b) Hall coefficient as a function of temperature with 10% error bar for $\text{CeO}_{0.9}\text{F}_{0.1}\text{FeAs}$ (■) and $\text{CeO}_{0.9}\text{F}_{0.1}\text{Fe}_{0.95}\text{Co}_{0.05}\text{As}$ (●). The straight line in figure (a) is a guide to eye and shows linearity.

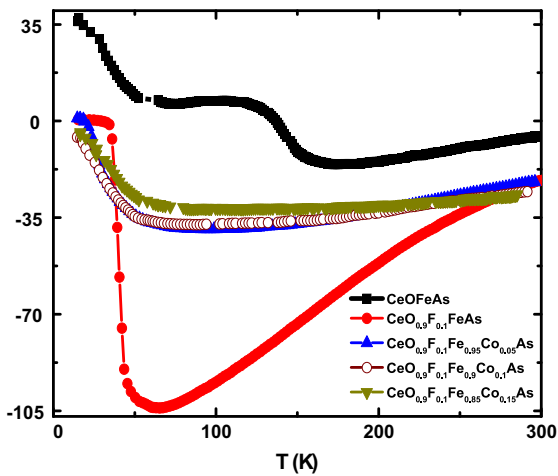


Fig. 5. The variation of thermoelectric power (S) with respect to temperature for $\text{CeO}_{0.9}\text{F}_{0.1}\text{Fe}_{1-x}\text{Co}_x\text{As}$ ($x = 0, 0.05, 0.10$ and 0.15) with respect to parent compound CeOFeAs .

fields for $\text{CeO}_{0.9}\text{F}_{0.1}\text{FeAs}$ and $\text{CeO}_{0.9}\text{F}_{0.1}\text{Fe}_{0.95}\text{Co}_{0.05}\text{As}$. From Fig. 6 it is clear that the T_c (onset) shifts weakly with magnetic field, but the zero resistivity temperature shifts much more rapidly to lower temperatures. Using a criterion of 90% and 10% of normal state resistivity (ρ_n), the upper critical field (H_{c2}) and the irreversibility field $H^*(T)$ were calculated. The H - T phase diagram for sample

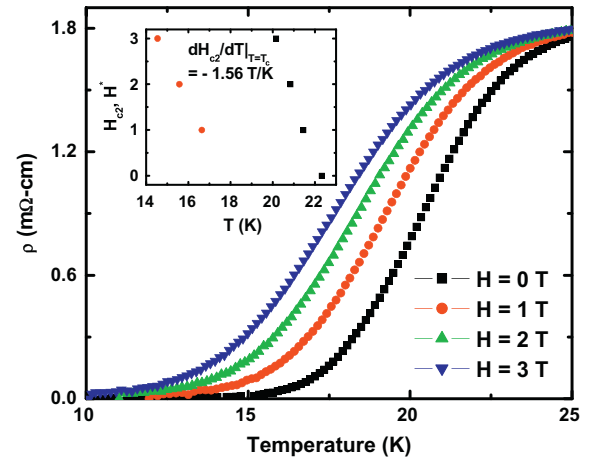


Fig. 6. Temperature dependence of the electrical resistivity of $\text{CeO}_{0.9}\text{F}_{0.1}\text{Fe}_{0.95}\text{Co}_{0.05}\text{As}$ with varying magnetic fields. Inset shows the temperature dependence of upper critical field (■) and irreversibility field (●) as a function of temperature.

$\text{CeO}_{0.9}\text{F}_{0.1}\text{Fe}_{0.95}\text{Co}_{0.05}\text{As}$ is shown in inset of Fig. 6. The zero field upper critical field $H_{c2}(0)$ is calculated using the Werthamer–Helfand–Hohenberg (WHH) formula [19]. Using the value of transition temperature (T_c) of 23.4 K, we find $H_{c2} = 25.3\text{ T}$. This value is smaller than the reported H_{c2} value ($\sim 94\text{ T}$) of $\text{CeO}_{0.9}\text{F}_{0.1}\text{FeAs}$ [10]. Using the value of $H_{c2}(0)$ we can also calculate the mean field Ginzberg–Landau coherence length $\xi_{ab} = (\Phi_0/2\pi H_{c2})^{1/2}$. Using $\Phi_0 = 2.07 \times 10^{-7}\text{ G cm}^2$ and the H_{c2} values, we obtain a coherence length of $\sim 36\text{ \AA}$ for $\text{CeO}_{0.9}\text{F}_{0.1}\text{Fe}_{0.95}\text{Co}_{0.05}\text{As}$ composition. This value is higher than that reported for sample $\text{CeO}_{0.9}\text{F}_{0.1}\text{FeAs}$ [10] and indicates that impurity scattering in the superconducting state does not increase with Co doping.

The dependence of the penetration depth is directly related to the anisotropy of the superconducting energy gaps [20]. Both in the fluorine-doped or oxygen-deficient FeAs based superconductors, most of the reports indicate a fully gapped Fermi surface (FS). Measurements of the London penetration depth, $\lambda(T)$, on $\text{NdO}_{0.9}\text{F}_{0.1}\text{FeAs}$ [21], $\text{La}_{0.8}\text{Th}_{0.2}\text{OFeAs}$ [22] and $\text{SmO}_{1-x}\text{F}_y\text{FeAs}$ [23] show an exponential temperature dependence of $\lambda(T)$ at low temperatures. In Fig. 7 we plot the penetration depth for the $x = 0.0$ and 0.05 composition. We have considered penetration depth data up

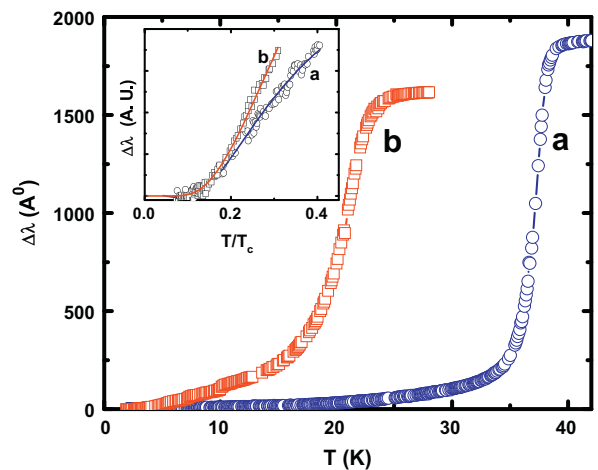


Fig. 7. Dependence of penetration depth for (a) $\text{CeO}_{0.9}\text{F}_{0.1}\text{FeAs}$ and (b) $\text{CeO}_{0.9}\text{F}_{0.1}\text{Fe}_{0.95}\text{Co}_{0.05}\text{As}$ up to the transition temperature attesting to the onset of bulk diamagnetism at T_c . The inset shows variation of penetration depth, $\Delta\lambda(T)$ for both the samples. The red and blue lines show the exponential fitting. (For interpretation of the references to colour in this figure legend, the reader is referred to the web version of this article.)

to $0.3T_c$ to ensure validity of the low temperature BCS expression for an isotropic s -wave state [20]

$$\Delta\lambda = \lambda(0) \times \sqrt{\frac{\pi\Delta(0)}{2T}} \exp[-\Delta(0)/T] \quad (1)$$

where $\Delta\lambda(T)$ is the difference between penetration depth at the temperature T and at lowest measurement temperature of 1.8 K. $\lambda(0)$ and $\Delta(0)$ are the zero temperature values of penetration depth and energy gap respectively. The absolute value of penetration depth is an approximation but the temperature dependence of change in penetration depth is accurate. The solid line in the Fig. 7 shows a curve fit to an isotropic single gap with the gap value of $\Delta_0/k_B = 22.3$ (gap ~ 1.9 meV) and 18 (gap ~ 1.6 meV) for $x = 0$ and $x = 0.05$ compositions respectively. Thus it appears that the gap value decreases with Co doping.

4. Conclusions

We have successfully synthesized cobalt-doped $\text{CeO}_{0.9}\text{F}_{0.1-x}\text{Fe}_{1-x}\text{Co}_x\text{As}$ ($x = 0.05, 0.1, \text{ and } 0.15$) compounds to study the interplay of charge carriers in both charge reservoir and charge carrier layers. The substitution of cobalt ion at the iron site in $\text{CeO}_{0.9}\text{F}_{0.1-x}\text{Fe}_{1-x}\text{Co}_x\text{As}$ compounds suppresses the transition temperature (T_c) and upper critical field (H_{c2}). Our penetration depth analysis indicates that both $\text{CeO}_{0.9}\text{F}_{0.1}\text{FeAs}$ and $\text{CeO}_{0.9}\text{F}_{0.1}\text{Fe}_{0.95}\text{Co}_{0.05}\text{As}$ follow S wave pairing symmetry with gap values of 1.9 and 1.6 meV respectively. We see increase in coherence length with increased disorder in the FeAs layer. The Hall and thermopower data show increase in charge carrier density on increasing the cobalt substitution at iron site.

Acknowledgements

A K G and S P thank D S T and U G C, Govt. of India for financial support. J P and S J S thank CSIR, Govt. of India, for fellowships.

References

- [1] I.I. Mazin, M.D. Johannes, Nat. Phys. 5 (2009) 41.
- [2] F. Bondino et al., Phys. Rev. Lett. 101 (2008) 267001.
- [3] C.N.R. Rao, A.K. Ganguli, Chem. Soc. Rev. 24 (1995) 1.
- [4] J. Zhao et al., Nat. Mater. 7 (2008) 953.
- [5] C. Wang et al., Phys. Rev. B 79 (2009) 054521.
- [6] J. Prakash, S.J. Singh, S. Patnaik, A.K. Ganguli, Solid State Commun. 149 (2009) 181; L.D. Zhao, D. Berardan, C. Bui, P. Gaudart, N. Dragoë, J. Phys.: Condens. Matter 22 (2010) 115701.
- [7] H. Yanagi et al., Phys. Rev. B 77 (2008) 224431.
- [8] A.S. Sefat et al., Phys. Rev. B 77 (2008) 174503.
- [9] S. Patnaik et al., Rev. Sci. Instrum. 70 (1999) 1494.
- [10] J. Prakash, S.J. Singh, S. Patnaik, A.K. Ganguli, Physica C 469 (2009) 82.
- [11] S.C. Lee et al., J. Phys. Soc. Jpn. 78 (2009) 043703.
- [12] J. Dai et al., 2009. Preprint at <<http://arxiv.org/abs/0901.2787v2>>.
- [13] G. Cao et al., Phys. Rev. B 79 (2009) 174505.
- [14] D. Barardan et al., Phys. Rev. B 81 (2010) 094506.
- [15] H. Yang et al., Phys. Rev. Lett. 101 (2008) 067001.
- [16] N.P. Ong, Physical Properties of High Temperature Superconductors, in: D.M. Ginsberg (Ed.), World Scientific, Singapore, 1990, p. 459.
- [17] A. Poddar et al., Physica C 469 (2009) 789.
- [18] D.J. Singh, M.H. Du, Phys. Rev. Lett. 100 (2008) 237003.
- [19] N.R. Werthamer, E. Helfand, P.C. Hohenberg, Phys. Rev. 147 (1966) 295.
- [20] A. Carrington et al., Physica C 385 (2003) 205.
- [21] R. Prozorov et al., Physica C 469 (2009) 582.
- [22] J. Prakash, S.J. Singh, S. Patnaik, A.K. Ganguli, J. Phys.: Condens. Matter 21 (2009) 175705.
- [23] L. Malone et al., Phys. Rev. B 79 (2009) 140501.